IMPLEMENTING MULTI-SCALE AGRICULTURAL INDICATORS EXPLOITING SENTINELS

VEGETATION FIELD DATA AND PRODUCTION OF GROUND-BASED MAPS:

"SAN FERNANDO SITE, CHILE" 19TH JANUARY 2015

ISSUE I1.01

EC Proposal Reference N° FP7-311766

Actual submission date : April 2015

Start date of project: 01.11.2012   Duration : 40 months

Name of lead partner for this deliverable: EOLAB

Book Captain: Consuelo Latorre (EOLAB)

Contributing Authors: Fernando Camacho (EOLAB)

Cristian Mattar, Andrés Santamaría-Artigas, Nicolas Leiva-Büchi (LAB-UC)

Project co-funded by the European Commission within the Seventh Framework Program (2007-2013)		
Dissemination Level		
PU	Public	**X**
PP	Restricted to other programme participants (including the Commission Services)	
RE	Restricted to a group specified by the consortium (including the Commission Services)	
CO	Confidential, only for members of the consortium (including the Commission Services)	

DOCUMENT RELEASE SHEET

Book Captain:	C. Latorre	Date: 01.02.2016	Sign.
Approval:	R. Lacaze	Date: 04.02.2016	Sign.
Endorsement:	M. Koleva	Date:	Sign.
Distribution:	Public		

CHANGE RECORD

Issue/Revision	Date	Page(s)	Description of Change	Release
	20.04.2015	All	First Issue	I1.00
	01.02.2016	34	Correct coordinates in Table 7	I1.01

TABLE OF CONTENTS

LIST OF FIGURES

LIST OF TABLES

LIST OF ACRONYMS

CEOS	Committee on Earth Observation Satellite
CEOS LPV	Land Product Validation Subgroup
DG AGRI	Directorate General for Agriculture and Rural Development
DG RELEX	Directorate General for External Relations (European Commission)
DHP	Digital Hemispheric Photographs
ECV	Essential Climate Variables
EUROSTATS	Directorate General of the European Commission
ESU	Elementary Sample Unit
FAPAR	Fraction of Absorbed Photo-synthetically Active Radiation
FAO	Food and Agriculture Organization
FCOVER	Fraction of Vegetation Cover
GCOS	Global Climate Observing System
GEO-GLAM	Global Agricultural Geo- Monitoring Initiative
GIO-GL	GMES Initial Operations - Global Land (GMES)
GCOS	Global Climate Observing System
GMES	Global Monitoring for Environment and Security
GPS	Global Positioning System
IMAGINES	Implementing Multi-scale Agricultural Indicators Exploiting Sentinels
JECAM	Joint Experiment for Crop Assessment and Monitoring
LAB-UC	*Laboratorio de Análisis de la Biosfera, Universidad de Chile*
LAI	Leaf Area Index
LDAS	Land Data Assimilation System
LUT	Look-up-table techniques
NAOMI	New AstroSat Optical Modular Instrument
PAI	Plant Area Index
PROBA-V	Project for On-Board Autonomy satellite, the V standing for vegetation.
RMSE	Root Mean Square Error
SPOT /VGT	*Satellite Pour l'Observation de la Terre* / VEGETATION
SLT	Solar Local Time
SSOT	*Sistema Satelital para la Observación de la Tierra*
TOC	Top of Canopy Reflectance
USGS	U.S. Geological Survey Science organization
UNFCCC	United Nations Framework Convention on Climate Change
UTM	Universal Transverse Mercator coordinates system
VALERI	Validation of Land European Remote sensing Instruments
WGCV	Working Group on Calibration and Validation (CEOS)

1. BACKGROUND OF THE DOCUMENT

1.1. EXECUTIVE SUMMARY

The Copernicus Land Service has been built in the framework of the FP7 geoland2 project, which has set up pre-operational infrastructures. ImagineS intends to ensure the continuity of the innovation and development activities of geoland2 to support the operations of the global land component of the GMES Initial Operation (GIO) phase. In particular, the use of the future Sentinel data in an operational context will be prepared. Moreover, IMAGINES will favor the emergence of new downstream activities dedicated to the monitoring of crop and fodder production.

The main objectives of ImagineS are to (i) improve the retrieval of basic biophysical variables, mainly LAI, FAPAR and the surface albedo, identified as Terrestrial Essential Climate Variables, by merging the information coming from different sensors (PROBA-V and Landsat-8) in view to prepare the use of Sentinel missions data; (ii) develop qualified software able to process multi-sensor data at the global scale on a fully automatic basis; (iii) complement and contribute to the existing or future agricultural services by providing new data streams relying upon an original method to assess the above-ground biomass, based on the assimilation of satellite products in a Land Data Assimilation System (LDAS) in order to monitor the crop/fodder biomass production together with the carbon and water fluxes;(iv) demonstrate the added value of this contribution for a community of users acting at global, European, national, and regional scales.

Further, ImagineS will serve the growing needs of international (e.g. FAO and NGOs), European (e.g. DG AGRI, EUROSTATS, DG RELEX), and national users (e.g. national services in agro-meteorology, ministries, group of producers, traders) on accurate and reliable information for the implementation of the EU Common Agricultural Policy, of the food security policy, for early warning systems, and trading issues. ImagineS will also contribute to the Global Agricultural Geo-Monitoring Initiative (GEO-GLAM) by its original agriculture service which can monitor crop and fodder production together with the carbon and water fluxes and can provide drought indicators, and through links with JECAM (Joint Experiment for Crop Assessment and Monitoring).

1.2. PORTFOLIO

The ImagineS portfolio contains global and regional biophysical variables derived from multi-sensor satellite data, at different spatial resolutions, together with agricultural indicators, including the above-ground biomass, the carbon and water fluxes, and drought indices resulting from the assimilation of the biophysical variables in the Land Data Assimilation System (LDAS).

The production in Near Real Time of the 333m resolution products, at a frequency of 10 days, using PROBA-V data is carried out in the Copernicus Global Land Service. It should start by covering Europe only, and be gradually extended to the whole globe.

Meanwhile, ImagineS will perform in parallel off-line production over demonstration sites outside Europe. The demonstration of high resolution (30m) products (Landsat-8 + PROBA-

V) will be done over demonstration sites of cropland and grassland in contrasting climatic and environmental conditions.

1.3. SCOPE AND OBJECTIVES

The main objective of this document is to describe the field campaign and ground data collected at San Fernando site - Chile and the up-scaling of the ground data to produce ground-based high resolution maps of the following biophysical variable:

- Leaf Area Index (LAI), defined as half of the total developed area of leaves per unit ground surface area (m^2/m^2). We focused on two different LAI quantities (for green elements):
  - ➢ The effective LAI (LAIeff) derived from the description of the gap fraction as a function of the view zenith angle. In addition, effective LAI measures derived at 57.5⁰ are also provided in the ground database.
  - ➢ The actual LAI (LAI) estimate corrected from the clumping index.
- Fraction of green Vegetation Cover (FCover), defined as the proportion of soil covered by vegetation, derived from the gap fraction between 0 and 10⁰ of view zenith angle.
- Fraction of Absorbed Photosynthetically Active Radiation (FAPAR), which is the fraction of the photosynthetically active radiation (PAR) absorbed by a vegetation canopy. PAR is the solar radiation reaching the canopy in the 0.4–0.7 μm wavelength region. We focused on the instantaneous FAPAR computed as the black-sky FAPAR at 10:00 SLT, which is the FAPAR under direct illumination conditions at a given solar position. In addition, two other quantities are provided in the ground database: daily integrated 'black-sky' FAPAR integrated over the day and the 'white-sky' FAPAR, which is the FAPAR under diffuse illumination conditions.

1.4. CONTENT OF THE DOCUMENT

This document is structured as follows:

- Chapter 2 provides an introduction to the field experiment.
- Chapter 3 provides the location and description of the site.
- Chapter 4 describes the ground measurements, including material and methods, sampling and data processing.
- Chapter 5 provides an evaluation of the sampling.
- Chapter 6 describes the production of high resolution ground-based maps, and the selected "mean" values for validation.

2. INTRODUCTION

Validation of remote sensing products is mandatory to guaranty that the satellite products meets the user's requirements. Protocols for validation of global LAIeff products are already developed in the context of Land Product Validation (LPV) group of the Committee on Earth Observation Satellite (CEOS) for the validation of satellite-derived land products (Fernandes et al., 2014), and recently applied to Copernicus global land products based on SPOT/VGT observation (Camacho et al., 2013). This generic approach is made of 2 major components:

- The indirect validation: including inter-comparison between products as well as evaluation of their temporal and spatial consistency
- The direct validation: comparing satellite products to ground measurements of the corresponding biophysical variables. In the case of low and medium resolution sensors, the main difficulty relies on scaling local ground measurements to the extent corresponding to pixels size. However, the direct validation is limited by the small number of sites, for that reason a main objective of ImagineS is the collection of ground truth data in demonstration sites.

The content of this document is compliant with existing validation guidelines (for direct validation) as proposed by the CEOS LPV group (Morisette et al., 2006); the VALERI project (http://w3.avignon.inra.fr/valeri/) and ESA campaigns (Baret and Fernandes, 2012). It therefore follows the general strategy based on a bottom up approach: it starts from the scale of the individual measurements that are aggregated over an elementary sampling unit (ESU) corresponding to a support area consistent with that of the high resolution imagery used for the up-scaling of ground data. Several ESUs are sampled over the site. Radiometric values over a decametric image are also extracted over the ESUs. This will be later used to develop empirical transfer functions for up-scaling the ESU ground measurements (e.g. Martínez et al., 2009). Finally, the high resolution ground based map will be compared with the medium resolution satellite product at the spatial support of the product.

One of the demonstration sites of ImagineS is located in San Fernando, Chile. In January, 2015 over this agricultural site, an intensive field campaign was conducted to characterize the vegetation biophysical parameters. The activities were carried out by EOLAB in collaboration with LAB-UC (*Laboratorio para el Análisis de la Biosfera, Universidad de Chile*).

Intensive Field Campaign: 19th - 20th of January 2015.

Contact:

LAB: Cristian Mattar – cmattar.lab@gmail.com
EOLAB: Fernando Camacho - fernando.camacho@eolab.es

Teams involved in field collection:

EOLAB: F. Camacho

LAB-UC: C. Mattar, A. Santamaría-Artigas, N. Leiva-Büchi (Figure 1).

Figure 1: LAB-UC team involved in the collection of ground data. Field campaign on 19th January, 2015 in San Fernando site (Chile).

3. STUDY AREA

3.1. LOCATION

"San Fernando" site is near to San Fernando city, the capital of the province of Colchagua, in central Chile and the second most populated urban center of the O'Higgins Region (see Table 1). This region is popularly known as the heart of Chilean agriculture. It is located in a fertile valley close to the Tinguiririca River, 12 km away from the reservoir Convento Viejo and Chimbarongo town. (Figure 2).
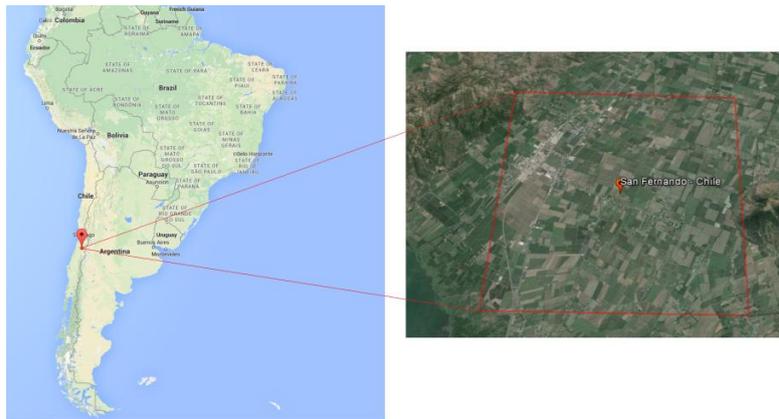
Figure 2: Location of San Fernando site, Chile.

Table 1: Coordinates and altitude of the test site (centre).

Site Center	
Geographic Lat/lon, WGS-84 (degrees)	Latitude = 34º 43' 23.88'' S Longitude = 71º 0' 5.42'' W
Altitude	320 m

3.2. DESCRIPTION OF THE TEST SITE

The study area is located in a valley. The climate is warm and temperate. There is a great deal of rainfall in San Fernando, even in the driest month. The climate is classified as oceanic climate by the Köppen-Geiger system. With an average of 20.6 °C, January is the warmest month. The lowest average temperatures in the year occur in July, when it is around 7.9 °C. The variation in temperatures throughout the year is 12.7 °C. The greatest amount of precipitation occurs in June, with an average of 217 mm, the precipitation varies 211 mm between the driest month (January) and the wettest month.

Ground measurements were conducted over selected fields located on a flat cropland area covered by annual crops. Ten different land cover types (i.e., raspberry, tobacco, blueberry, corn, beans, alfalfa) were characterized during the campaign. Figure 3 shows some examples of these land cover types.

a) Beans   b) Raspeberry   c) Corn   d)Tobacco

e) Pepper
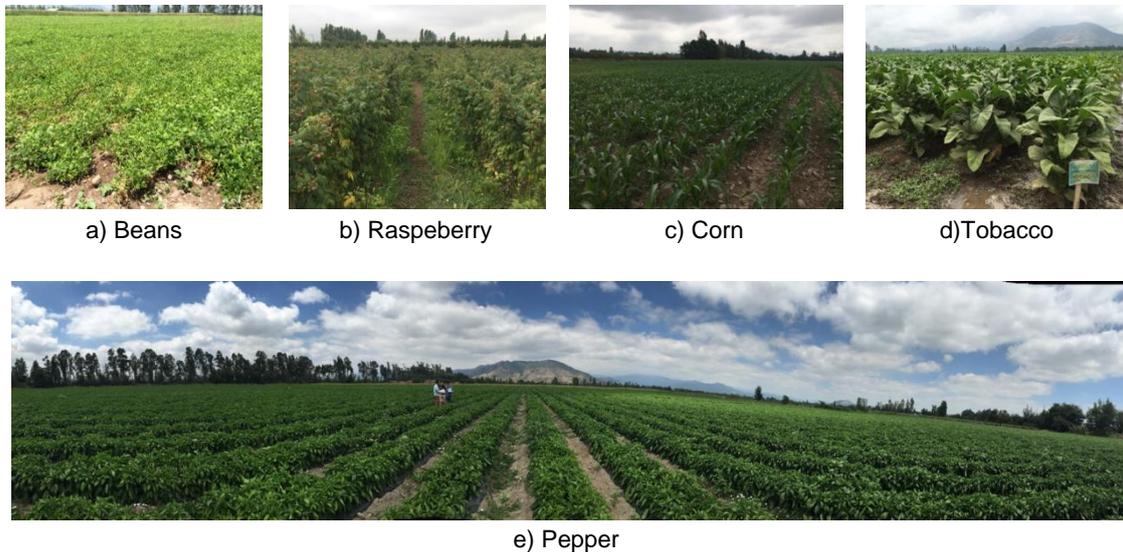
Figure 3: Examples of the different San Fernando site (Chile) during the intensive field campaign in 19th January, 2015.

The image selected for the up-scaling belongs to the chilean FASAT-C satellite, acquired on 18th January 2015, the previous day to the field campaign. Figure 4 shows a RGB false color composition, where some clouds can be observed on the top of the image.
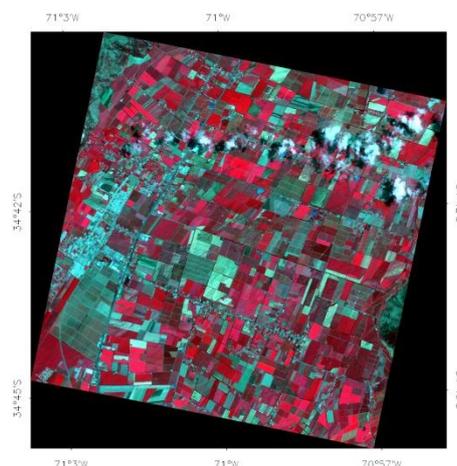
Figure 4: False color composition (RGB: NIR-Red-Green) FASAT-C TOA Reflectance image over the 10x10 km² study area (18th, January 2015).

4. GROUND MEASUREMENTS

The ground measurement database reported here was acquired by EOLAB.

Additional hemispheric photographs, standard digital photos and soil moisture measurements were also taken to characterize the fields by the LAB.

4.1. MATERIAL AND METHODS

4.1.1 Digital Hemispheric Photographs (DHP)

Digital hemispherical photos allow the calculation of LAI, FAPAR and FCOVER measuring gap fraction through an extreme wide-angle camera lens (i.e. 180º) (Weiss et al., 2004). It produces circular images that record the size, shape, and location of gaps, either looking upward from within a canopy or looking downward from above the canopy. Two hemispherical cameras were used during the campaign, both equipped with a full-circle hemispherical lens.

The hemispherical photos acquired during the field campaign were analyzed semi-automatically to compute the biophysical variables. The processing was conducted by the same operator for all the images with the Can Eye software versions: v.6.312 and v.6.4 (developed by INRA http://www6.paca.inra.fr/can-eye) to derive LAI, FAPAR and FCOVER. It is based on a RGB colour classification of the image to discriminate vegetation elements from background (i.e., gaps). This approach allows exploiting downward-looking photographs for short canopies (background = soil) as well as upward-looking photographs for tall canopies (background = sky). CAN-EYE software processes simultaneously up to 20 images acquired over the same ESU. Note that our images were acquired with similar illumination conditions to limit the variation of colour dynamics between images.

The processing is achieved in 3 main steps (Weiss et al., 2004). First, image pre-processing is performed, which includes removing undesired objects (e.g. operator, sun glint) and image contrast adjustments to ensure a better visual discrimination between vegetation elements and background. Second, an automatic classification (k-means clustering) is applied to reduce the total number of distinctive colours of the image to 324 which is sufficient to ensure accurate discrimination capacities while keeping a small enough number of colours to be easily manipulated. Finally, a default classification based on predefined colour segmentation is first proposed and then iteratively refined by the user. The allocation of the colours to each class (vegetation elements versus background) is the most critical phase that needs to be interactive because colours depend both on illumination conditions and on canopy elements. At the end of this process a binary image, background versus vegetation elements (including both green and non-green elements) is obtained.

The CAN-EYE software computes biophysical variables from gap fraction as follows:

Effective LAI (LAIeff): Among the several methods described in Weiss et al (2004), the effective LAI estimation in the CAN-EYE software is performed by model inversion. The effective LAI is estimated from the Plant Area Index (PAI) which is the variable estimated by CAN-EYE, as no distinction between leaves or other plant elements are made from the gap fraction estimates. PAI is very close to the effective LAI for croplands when pictures are taken downward looking, whereas larger discrepancies are expected for forest when pictures are taken upward looking. Effective LAI is directly retrieved by inverting Eq. (1) (Poisson model) and assuming an ellipsoidal distribution of the leaf inclination using look-up-table (LUT) techniques.

$$P_0(\theta_v, \varphi_v) = e^{-N \cdot (\theta_v, \varphi_v)} = e^{-G \cdot (\theta_v, \varphi_v) \cdot \frac{LAI_{eff}}{\cos(\theta_v)}}$$ Eq. (1)

A large range of random combinations of LAI (between 0 and 10, step of 0.01) and ALA (Average Leaf Angle)(10° and 80°, step of 2°) values is used to build a database made of the corresponding gap fraction values (Eq.1) in the zenithal directions defined by the CAN-EYE user (60° for the DHP collection in this field campaign). The process consists then in selecting the LUT element in the database that is the closest to the measured P_0. The distance (cost function C_k) of the kth element of the LUT to the measured gap fraction is computed as the sum of two terms. The first term computes a weighted relative root mean square error between the measured gap fraction and the LUT one. The second term is the regularization term that imposes constraints to improve the PAI estimates. Two equations are proposed for the second "regularization" term:

(1) constraint used in CAN-EYE V5.1 on the retrieved ALA values that assume an average leaf angle close to $60^o \pm 03^o$, and

(2) constraint used in CAN-EYE V6.1 on the retrieved PAI value that must be close from the one retrieved from the zenithal ring at 57°. This constraint is more efficient, but it can be computed only when the 57° ring is available (i.e., COI≥60º)

The software also proposed other ways of computing PAI and ALA effective using Miller's formula (Miller, 1967) which assumed that gap fraction only depends from view zenith angle. Furthermore, the CAN-EYE makes an estimation using the Welles and Norman (1991) method used in LAI-2000 for 5 rings. These LAI2000-like estimates were not used here as are based on the same Miller's formula but using limited angular sampling.

LAI: The actual LAI that can be measured only with a planimeter with however possible allometric relationships to reduce the sampling, is related to the effective leaf area index through:

$$LAI_{eff} = \lambda_0 \cdot LAI$$ Eq. (2)

where λ_0 is the clumping index. In CAN-EYE, the clumping index is computed using the Lang and Xiang (1986) logarithm gap fraction averaging method, although some uncertainties are associated to this method (Demarez et al., 2008). The principle is based on the assumption that vegetation elements are locally assumed randomly distributed. Values of clumping index

given by CAN_EYE are in certain cases correlated with the size of the cells used to divide photographs.

Two versions of CAN-EYE were used, v6.3.1.2 and v6.4. Results from version 6.4 were selected due to the more realistic classification over shadow areas and cloudy sky. As the CAN-EYE software provides different results (CEV6.1, CEV5.1 and Miller's) for LAI and LAIeff variables, an average of the three LAI values were provided as ground estimate for LAIeff, and the mean value between CEV6.1 and CEV5.1 for LAI. The standard deviation of the different considered methods was reported as the uncertainty of the LAI estimate (see associated 20150119_VGM_SanFernando.xls file).

FCOVER is retrieved from gap fraction between 0 to 10°.

$$FCOVER = 1 - P_0 \cdot (0 - 10°) \hspace{3cm} \text{Eq. (3)}$$

FAPAR: As there is little scattering by leaves in that particular spectral domain due to the strong absorbing features of the photosynthetic pigments, FAPAR is often assumed to be equal to FIPAR (Fraction of Intercepted Photosynthetically Active Radiation), and therefore to the gap fraction. The actual FAPAR is the sum of two terms, weighted by the diffuse fraction in the PAR domain: the 'black sky' FAPAR that corresponds to the direct component and the 'white sky' or the diffuse component.

The instantaneous "Black-sky FAPAR" (FPAR[BS]) is given at a solar position (date, hour and latitude). Depending on latitude, the CAN EYE software computes the solar zenith angle every solar hour during half the day (there is symmetry at 12:00). The instantaneous FAPAR is then approximated at each solar hour as the gap fraction in the corresponding solar zenith angle:

$$FAPAR^{BS}(\theta_S) = 1 - P_0 \cdot (\theta_S) \hspace{3cm} \text{Eq. (4)}$$

The daily integrated black sky or direct FAPAR is computed as the following:

$$FAPAR_{Day}^{BS} = \frac{\int_{sunset}^{sunrise} cos(\theta_S) \cdot [1 - P_0 \cdot (\theta_S)] \cdot d\theta}{\int_{sunset}^{sunrise} cos(\theta_S) \cdot d\theta} \hspace{2cm} \text{Eq. (5)}$$

In this report, we focused on the instantaneous black-sky FAPAR measured at 10:00 SLT for up-scaling. Daily integrated FAPAR and White-sky FAPAR are also provided in the ground database.

4.1.2 Soil measurements

Soil moisture measurements were acquired with a Hydrosense II, a portable, handheld device manufactured by Campbell Scientific, inc. The Handheld TDR HydroSense II measures volumetric water content of soil. The major components of the system are the display, the sensor, and the software. It presents a Volumetric Water Content Accuracy of 3% typical and a Volumetric Water Content resolution greater than 0.05%. This dataset should be requested to LAB-UC.

4.2. SPATIAL SAMPLING SCHEME

A pseudo-regular sampling was used within each ESU of approximately 20x20 m^2. The centre of the ESU was geo-located using a GPS. A total of 40 ESUs were characterized (Table 2). The number of hemispherical photos per ESU ranges between 11 and 15 for processing with CAN-EYE and a pair for visual inspection classification. The 40 ESUs are mainly located over corn and tobbaco fields that are the main crops in the area.

The sampling scheme for the DHP collection is shown in Figure 5. The ground measurements are spread across fields of pepper, beans, alfalfa, blueberry, raspberry, corn, tobacco, potato, bare areas and an apple tree plantation. Table 2 summarizes the number sampling units (ESUs) and DHPs collected per each crop type acquired during the field campaigns.

Figure 5: Distribution of the sampling units (ESUS) over the study area. DHP sampling over 5x5 km^2 FASAT-C TOA RGB, GoogleEarth. San Fernando, Chile. 19th January, 2015.

Table 2: Cardinality of DHP measurements, globally and for each land cover class in San Fernando site (Chile).

ESU internal code	Number of ESU's	
	Field Campaign (19th and 20th of January, 2015)	
	Nº ESUs	Nº DHPs
Raspeberry	3	37
Tobacco	10	125
Blueberry	2	25
Apple Tree	1	20
Bare soil	1	4
Pepper	3	37
Corn	12	147
Beans	4	48
Alfalfa	3	37
Potato	1	11
Total	40	491

4.3. GROUND DATA

4.3.1 Data processing

The software CAN-EYE versions V6.3.12 and V6.4 were used to process the DHP images. Figure 6 shows some examples of DHP over different land cover types.

| a) Alfalfa | b) Tobacco | c) Corn | d) Apple Tree |

Figure 6: Digital Hemispherical Photographs acquired in San Fernando site, (Chile) during the intensive campaign of 19th January 2015.

Downward measurements were conducted on most of the fields. Upward measurements were taken instead on Raspberry and on the field of corn due to the stage of the crop.

For the Apple tree plantation (ESU #13) with understory and overstory, hemispherical images were acquired upward looking (overstory) and downward looking (understory). The two sets of acquisitions were processed separately to derived LAI (effective and true), FAPAR and FCOVER (Latorre et al., 2014).

Figure 7 to Figure 9 show the comparison between the two versions of CAN-EYE software. The results are very similar, although the new version is more accurate due to the analyst is able to force an area to belong to a given class. ESUs which presented shadow over vegetation and cloudy sky zones were better discriminated with this option (v.6.4).
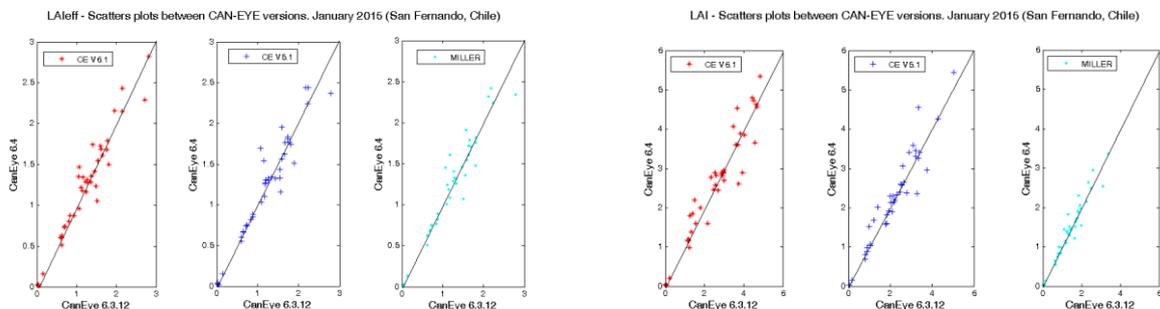
Figure 7: Comparison between CAN-EYE versions, V6.3.12 and V6.4. San Fernando site, (Chile) during the intensive campaign of 19th January 2015.

FAPAR - Scatters plots between CAN-EYE versions. January 2015 (San Fernando, Chile)
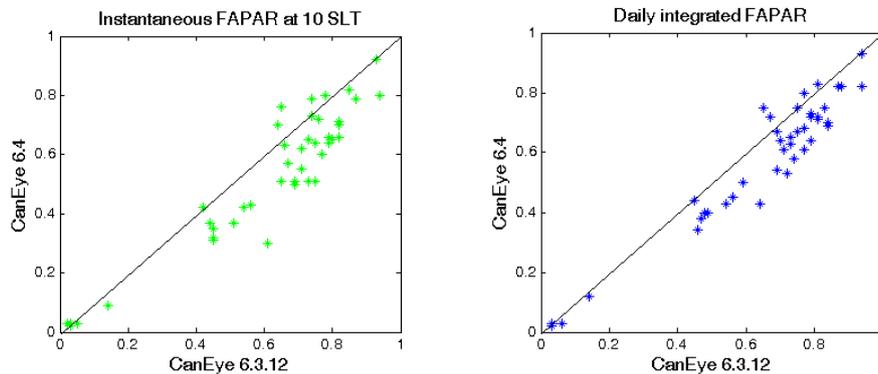
Figure 8: Comparison between CAN-EYE versions, V6.3.12 and V6.4. San Fernando site, (Chile) during the intensive campaign of 19th January 2015.

For the FAPAR variable a systematic bias was obtained with lower values for 6.4 version, whereas the results for FCOVER (Figure 9) were found very consistent.

FCOVER - Scatters plots between CAN-EYE versions. January 2015 (San Fernando, Chile)
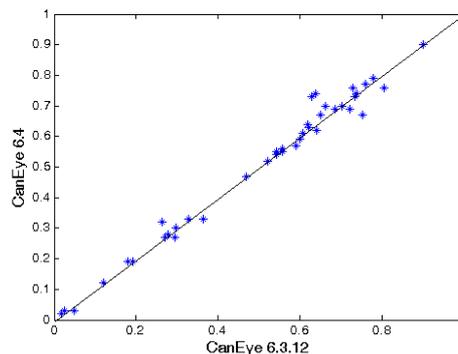
Figure 9: Comparison between CAN-EYE versions, V6.3.12 and V6.4. San Fernando site, (Chile) during the intensive campaign of 19th January 2015.

Effective LAI values were calculated with the average of three different estimations (CEV6.1, CEV5.1 and Miller's) as described in Section 4.1. These estimations were found very consistent for the effective LAI (Figure 10), and the averaged value was used for determining the empirical transfer function. However, for the actual LAI values, large dispersion was found between CEV6.1 or CEV5.1 and Miller's method. As the Miller's method only uses zenithal angles, we have computed an averaged LAI value using the two estimates based on the Can-Eye approaches (Figure 11).
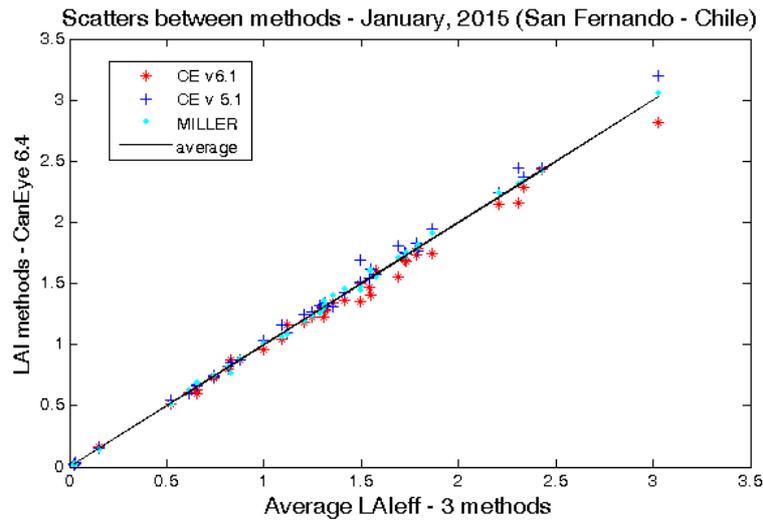
Figure 10: LAIeff values derived from different methods (CEV5.1, CEV6.1 and Miller´s formula) as a function of the averaged value. San Fernando site (Chile), 19th January, 2015.
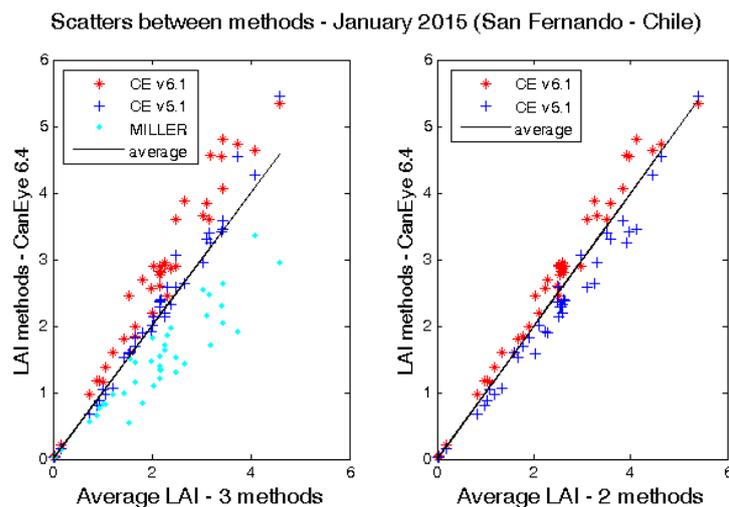
Figure 11: LAI values derived from different methods as a function of the averaged value. San Fernando site (Chile), 19th January, 2015. Left side: CEV5.1, CEV6.1. and Miller´s formula. Right side: CEV5.1 and CEV6.1.

Figure 12 shows the inter-comparison between FAPAR with LAI estimations and FAPAR versus FCOVER estimations. As can be observed, the relation between variables follows the expected exponential trend between LAI and FAPAR, and the linear trend between FCover and FAPAR. However, some dispersion between FAPAR and FCOVER was observed for some cover types as peppers, with larger FCOVER values than FAPAR values. This behavior is analyzed below.
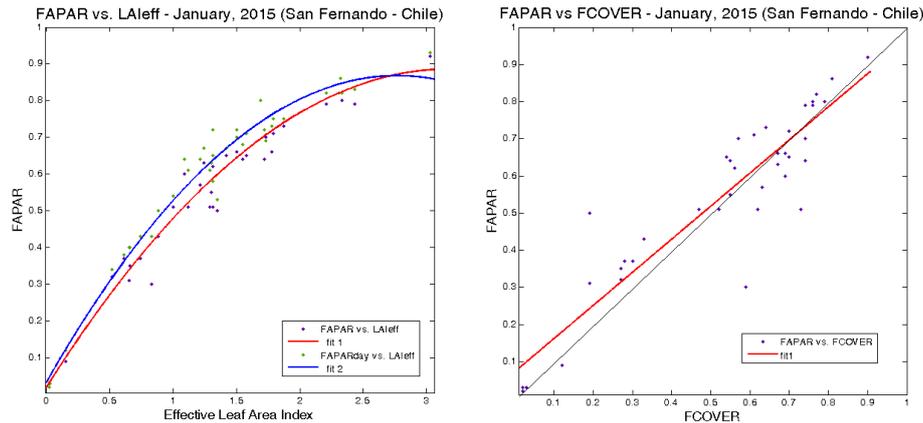
Figure 12: Intercomparison of the measured biophysical variables. FAPAR versus LAIeff (Left side) and FAPAR versus FCOVER (Right side). San Fernando site (Chile) 19th January, 2015.

- **Inconsistencies detected between FAPAR and FCOVER for crops with wide rows**

For several crops displaying a row distribution such as for pepper (Figure 13) we have detected an overestimation of the FCOVER as compared to the FAPAR up to 0.2. As the FAPAR is approximated by the FIPAR (1 minus gap fraction in the direction of the sun zenith angle) it must be larger than FCOVER (1 minus gap fraction at nadir). This overestimation can be explained due to the sampling and the low angular field of view used for computation of the FCOVER (0-10º). As can be observed in Figure 13, almost for all the 12 shots the vegetated row falls in the middle of the digital photo, which implies a high fraction of vegetation cover. However, for the computation of the FAPAR the gap fraction is computed at larger zenithal angles (~30º) where both soil and vegetation rows are correctly detected. This effect was observed for several ESUs of Pepper and Tobacco, both with wide rows of soil and vegetation.
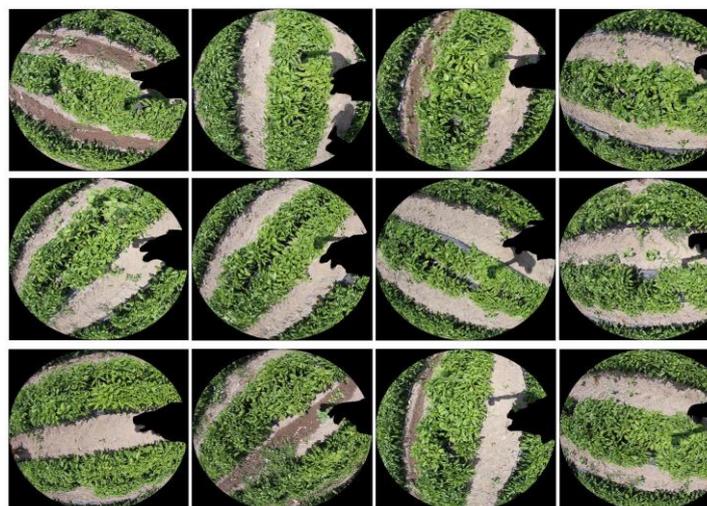
Figure 13: Example DHPs and average image computed with CAN-EYE for the ESU#15 of pepper. San Fernando site (Chile) 19th January, 2015.

In conclusion, the FCOVER is larger than the FAPAR due to the fact that the sampling for FCOVER does not capture well the variability within the ESU. For this type of crops, it should be convenient to perform additional standard digital photos to capture within the footprint of the camera the existing variability of the crop.

4.3.2 Content of the Ground Dataset

Each ESU is described according to a standard format. The header of the database is shown in Table 3.

Table 3: The Header used to describe ESUs with the ground measurements.

Column	Var.Name		Comment
1	Plot #		Number of the field plot in the site
2	Plot Label		Label of the plot in the site
3	ESU #		Number of the Elementary Sampling Unit (ESU)
4	ESU Label		Label of the ESU in the campaign
5	Northing Coord.		Geographical coordinate: Latitude (º), WGS-84
6	Easting Coord.		Geographical coordinate: Longitude (º), WGS-84
7	Extent (m) of ESU (diameter)		Size of the ESU [1]
8	Land Cover		Detailed land cover
9	Start Date (dd/mm/yyyy)		Starting date of measurements
10	End Date (dd/mm/yyyy)		Ending date of measurements
11	Products*	Method	Instrument
12		Nb. Replications	Number of Replications
13		Products*	Methodology
14		Uncertainty	Standard deviation

*LAIeff, LAI, FAPAR and FCOVER

Figure 14 to Figure 16 show the measurements obtained during the field experiment per land cover type and per ESU. The figures on the top show a distribution grouped by land cover, and the bottom ones the distribution by ESUs.

LAIeff shows minimum values for 0.02 (Corn ESUs C7 to C9) and maximum ranging between 2 and 2.5 (Beans and Apple tree) (Figure 14). The LAI shows a similar distribution although with higher values due to the correction of the clumping. Maximum values are reported for apple tree, tobacco and beans.

FAPAR instantaneous at 10:00 SLT values are lower than 0.85 (Figure 15), with minimum values for potato (0.11) and corn (0.02), and maximum for beans, alfalfa and Apple tree.
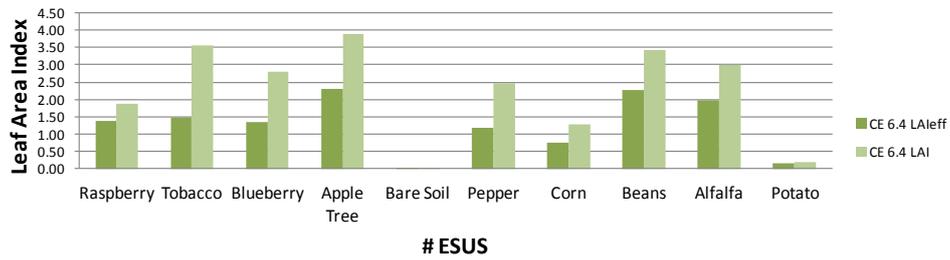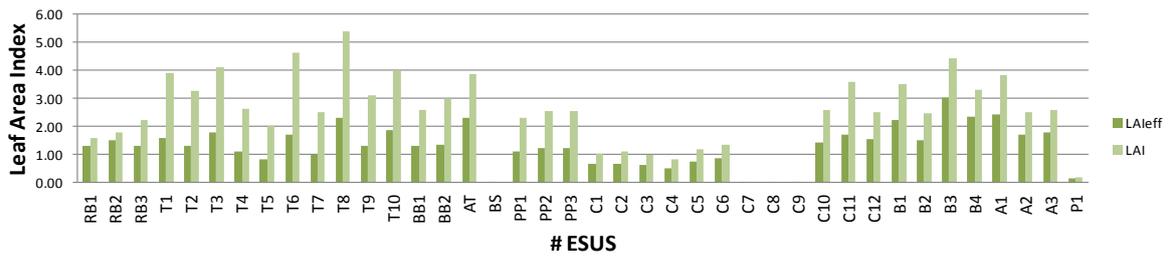
Figure 14: LAIeff and LAI measurements acquired in San Fernando site (Chile), during the campaign of 19th of January 2015. Top: Distribution by land cover types. Bottom: Distribution by ESUs.
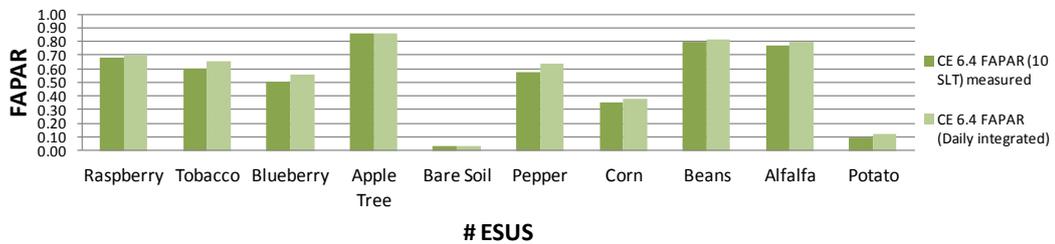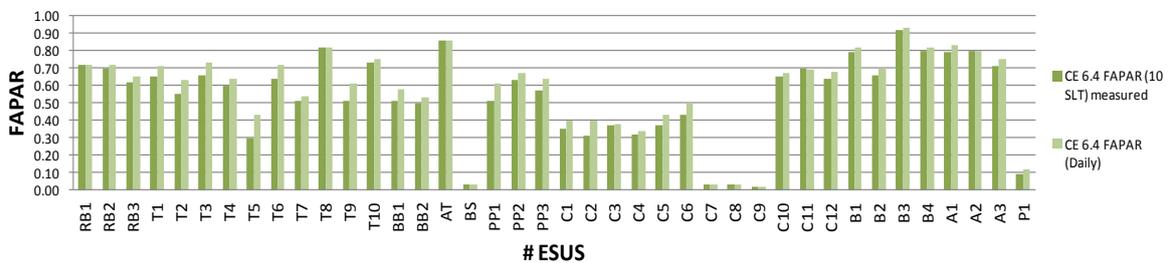
Figure 15: As in Figure 14 for FAPAR (instantaneous black-sky 10:00 SLT and daily integrated values).

For the FCOVER variable (Figure 16) a similar variability than for FAPAR is observed. Apple tree, beans and alfalfa measurements present the maximum values (up to 0.8). FCOVER shows values ranging from 0.1 (Potato) to 0.81 (Apple tree plantation). Raspberry, apple tree and some corn ESUs were acquired upward looking due to the plant height.
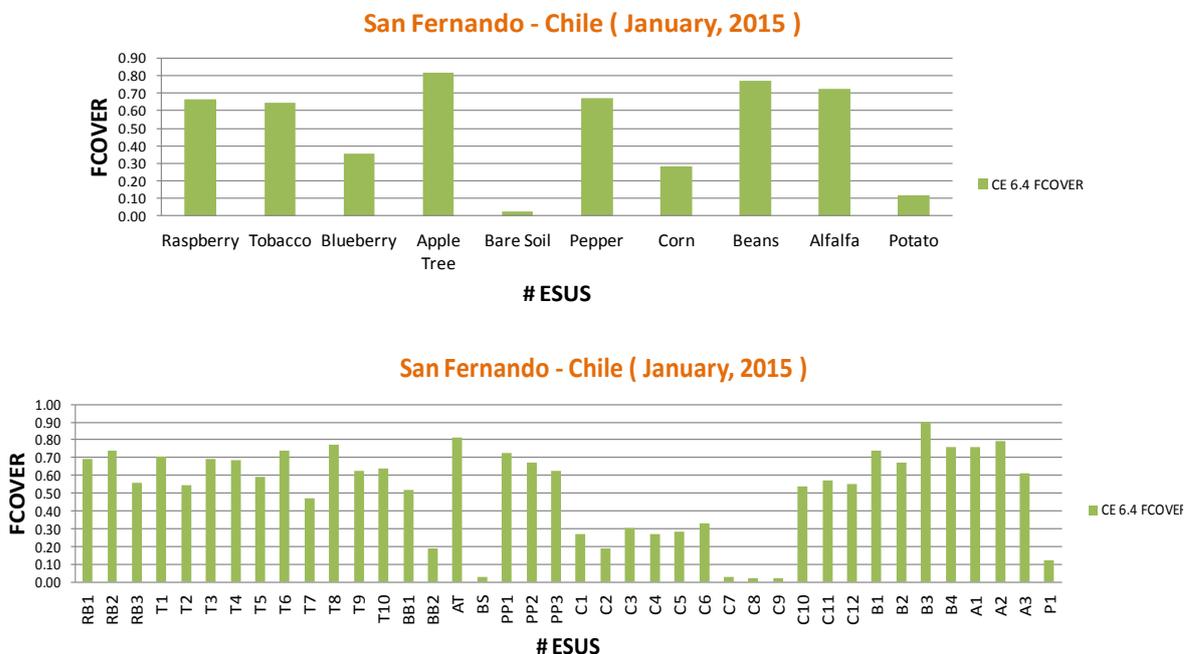
Figure 16: As in Figure 14 for FCOVER.

Figure 17 shows the distribution of the measured variables. For the effective LAI, the largest frequencies are observer around 1.5, and around 3 for LAI. For FAPAR and FCOVER, the higher frequencies are around 0.7.
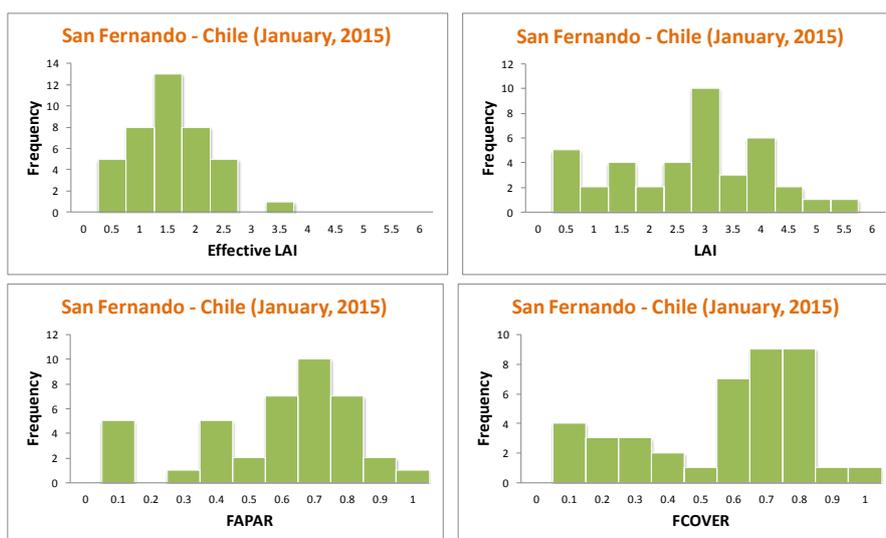
Figure 17: Distribution of the measured biophysical variables over the ESUs. San Fernando site, during the campaign of 19th January, 2015.

5. EVALUATION OF THE SAMPLING

5.1. EVALUATION BASED ON NDVI VALUES

The sampling strategy is evaluated using the FASAT-C image by comparing the NDVI distribution over the site with the NDVI distribution over the ESUs (Figure 18). As the number of pixels is drastically different for the ESU and whole site (WS) it is not statistically consistent to directly compare the two NDVI histograms. Therefore, the proposed technique consists in comparing the NDVI cumulative frequency of the two distributions by a Monte-Carlo procedure which aims at comparing the actual frequency to randomly shifted sampling patterns. It consists in:

1. computing the cumulative frequency of the N pixel NDVI that correspond to the exact ESU locations; then, applying a unique random translation to the sampling design (modulo the size of the image)

2. computing the cumulative frequency of NDVI on the randomly shifted sampling design

3. repeating steps 1 and 2, 199 times with 199 different random translation vectors.

This provides a total population of N = 199 + 1(actual) cumulative frequency on which a statistical test at acceptance probability 1 - α = 95% is applied: for a given NDVI level, if the actual ESU density function is between two limits defined by the $N\alpha / 2$ = 5 highest and lowest values of the 200 cumulative frequencies, the hypothesis assuming that WS and ESU NDVI distributions are equivalent is accepted, otherwise it is rejected.

Figure 18 shows that the NDVI distribution of San Fernando – January, 2015 campaign is good over the whole site (comprised between the highest and lowest cumulative frequencies).
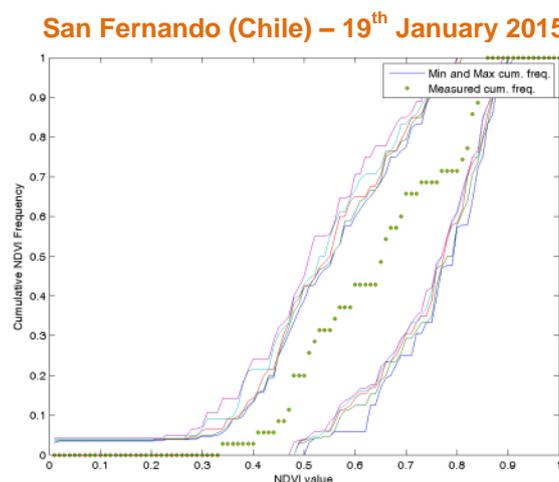
Figure 18: Comparison of NDVI distribution between ESUs and over the whole image. Field campaign (19th January, 2015), San Fernando site (Chile).

5.2.   EVALUATION BASED ON CONVEX HULL: PRODUCT QUALITY FLAG.

The interpolation capabilities of the empirical transfer function used for up-scaling the ground data using decametric images is dependent of the sampling (Martinez et al., 2009). A test based on the convex hulls was also carried out to characterize the representativeness of ESUs and the reliability of the empirical transfer function using the different combinations of the selected bands of the FASAT-C TOA image. A flag image is computed over the TOA reflectance, for the band combination used for generating the empirical biophysical maps: NIR-Red-Green (NRG) was selected for all products derived from FASAT-C imagery (see Section 6.2 for details). The result on convex-hulls can be interpreted as:

● pixels inside the 'strict convex-hull': a convex-hull is computed using all the FASAT-C TOA reflectance corresponding to the ESUs belonging to the class. These pixels are well represented by the ground sampling and therefore, when applying a transfer function the degree of confidence in the results will be quite high, since the transfer function will be used as an interpolator;

● pixels inside the 'large convex-hull': a convex-hull is computed using all the reflectance combinations (± 5% in relative value) corresponding to the ESUs. For these pixels, the degree of confidence in the obtained results will be quite good, since the transfer function is used as an extrapolator (but not far from interpolator);

● pixels outside the two convex-hulls: this means that for these pixels, the transfer function will behave as an extrapolator which makes the results less reliable. However, having a priori information on the site may help to evaluate the extrapolation capacities of the transfer function.

Figure 19 shows the results of the Convex-Hull test (i.e., Quality Flag images) for the San Fernando site over the 5x5 km^2 study area. The strict and large convex-hulls are high around the test site for the largest zone, 77% for the NRG combination over FASAT-C image (Table 4). Note that the pixels flagged as of lower quality (i.e. where the transfer function behaves as extrapolator) correspond in most cases to bare soil areas that were not sampled during the field experiment.

Table 4: FASAT-C image. Percentages over the two areas over the test site of San Fernando (Chile).Convex hull values: 0=extrapolation of TF, 1=strict convex hull and 2=large convex hull).

Field Campaign	Quality Flags (%)		
DATE	19th January, 2015		
NRG – FASAT-C	5x5 km^2		
Convex hull	0	1	2
values	23%	63%	14%

San Fernando site – Chile 19th January, 2015
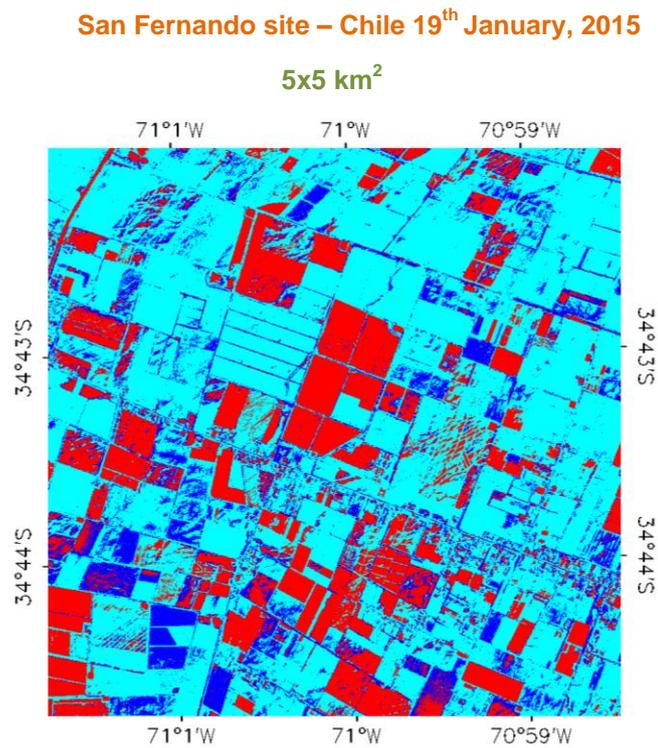
5x5 km[2]

Figure 19: Convex Hull test over 5x5 km[2] area. Clear and dark blue correspond to the pixels belonging to the 'strict' and 'large' convex hulls. Red corresponds to the pixels for which the transfer function behaves as extrapolator. San Fernando - Chile, 19th January 2015.

6. PRODUCTION OF GROUND-BASED MAPS

6.1. IMAGERY

FASAT-C is the first high spatial resolution mission operated by the Chilean Air Force. The SSOT (*Sistema Satelital para la Observación de la Tierra*; referred hereafter as FASAT-C) was launched on December 16th, 2011 (Mattar et al., 2014)

The FASAT-C image was acquired the 18th January 2015 by the pushbroom imager NAOMI-1 (New AstroSat Optical Modular Instrument). Three spectral bands were selected from 528 nm to 881 nm wavelengths with a nadir ground sampling distance of 5.8 m (multi-spectral bands) with a nominal swath width of 10 km. It has a heliosynchronous orbit at an altitude of 6290 km with an inclination of 97.8⁰. The satellite has a revisit time of 3-5 days with a viewing angle between ±30⁰, and a 37 days revisit time with a nadir view angle. (See Table 5 for acquisition properties).

Table 5: Acquisition properties of FASAT-C data used for retrieving high resolution maps.

FASAT-C TOA summary properties	
Platform / Instrument	NAOMI-1
Spectral Range selected	B2(green) : 0.528-0.588 µm B3(red) : 0.625-0.695 µm B4(NIR) : 0.758-0.881 µm
19th January 2015 campaign	
Acquisition date	2015.01.18

6.2. THE TRANSFER FUNCTION

6.2.1 The regression method

If the number of ESUs is enough, multiple robust regression 'REG' between ESUs reflectance and the considered biophysical variable can be applied (Martínez et al., 2009): we used the 'robustfit' function from the Matlab statistics toolbox. It uses an iteratively re-weighted least squares algorithm, with the weights at each iteration computed by applying the bi-square function to the residuals from the previous iteration. This algorithm provides lower weight to ESUs that do not fit well.

The results are less sensitive to outliers in the data as compared with ordinary least squares regression. At the end of the processing, two errors are computed: weighted RMSE (RW) (using the weights attributed to each ESU) and cross-validation RMSE (RC) (leave-one-out method).

As the method has limited extrapolation capacities, a flag image for each transfer function (Figure 19), are included in the ground based maps in order to inform the users on the reliability of the estimates.

6.2.2 Band combination

Figure 20 shows the errors (RW, RC) obtained for the several band combinations using TOA reflectance. Attending specifications of lower errors and maximum sensitivity to LAI, it has been chosen for FASAT-C maps: band 2 (Green), band 3(Red) and band 4 (NIR) combination (NRG). This combination presents less saturation and the most linear response. These combinations on reflectance were selected since they provide a good compromise between the low cross-validation RMSE, the weighted RMSE (lowest value) and the number of rejected points, but also considering the better sensitivity to the ground measurement.

San Fernando site – Chile 19th January, 2015
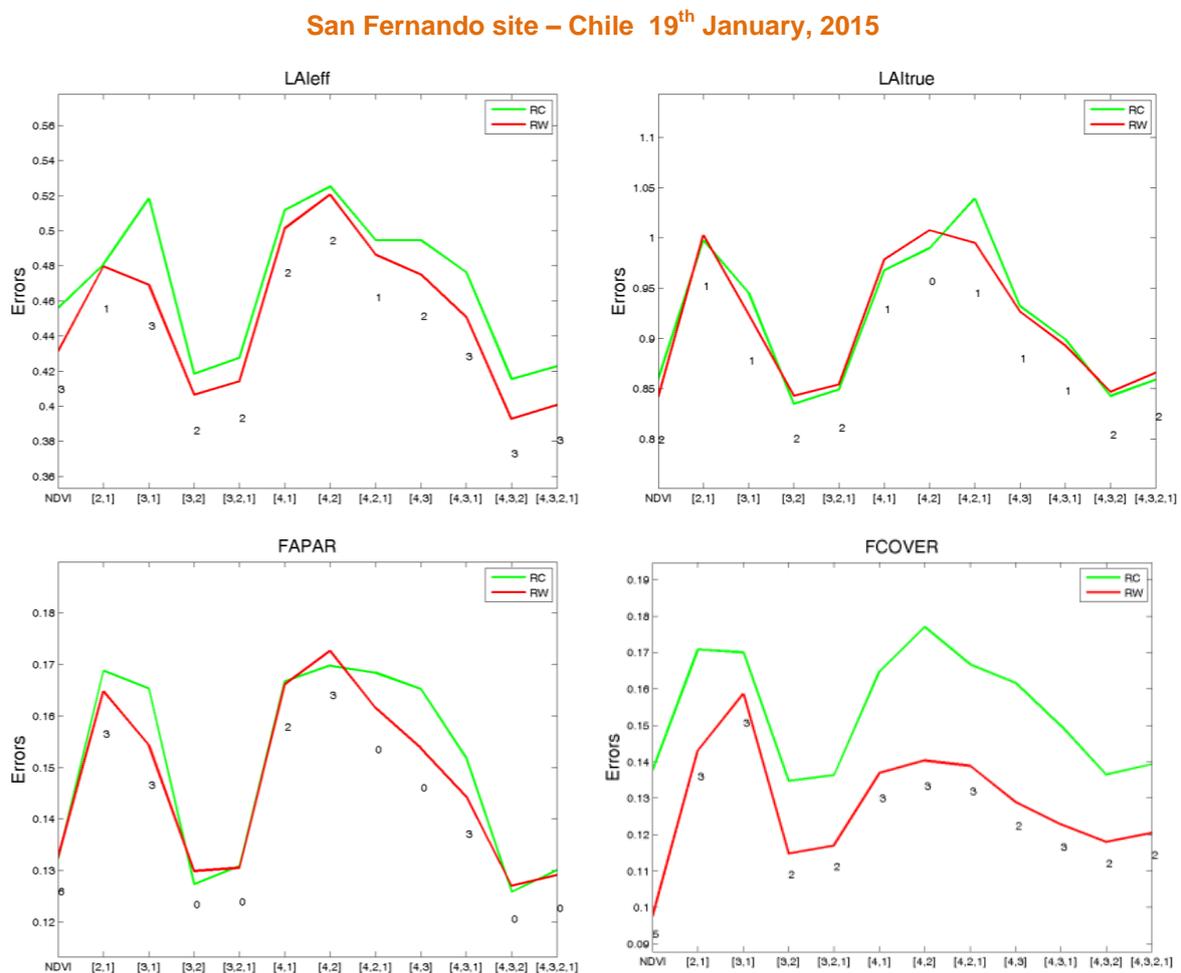
Figure 20: FASAT-C TOA. Test of multiple regressions (TF) applied on different band combinations. Band combinations are given in abscissa (1=Blue, 2=Green, 3=Red and 4=NIR).

6.2.3 The selected Transfer Function

The applied transfer function is detailed in Table 6, along with its weighted and cross validated errors.

Table 6: Transfer function applied to the whole site over FASAT-C image for LAIeff, LAI, FAPAR daily integrated and FCOVER. RW (weighted RMSE), RC (cross-validation RMSE).

Variable	Band Combination	RC	RW
	FASAT-C Transfer Function		
LAIeff	-0.3561277 -1.4984985·(NIR) -36.940304·(Red) + 69.476864·(Green)	0.42	0.39
LAI	-0.0172277 -1.4058761·(NIR) -58.303657·(Red) + 101.86870 ·(Green)	0.84	0.85
FAPAR	-0.1147007 -0.4757013 ·(NIR) -12.997326·(Red) + 24.749043·(Green)	0.12	0.13
FCOVER	0.0059084 -0.1036641·(NIR) -10.336793 ·(Red) + 17.846122·(Green)	0.13	0.12

Figure 21 shows scatter-plots between ground observations and their corresponding transfer function (TF) estimates for the selected bands combinations. A good correlation is observed for the products with points distributed along the 1:1 line and no bias, but some scattering.
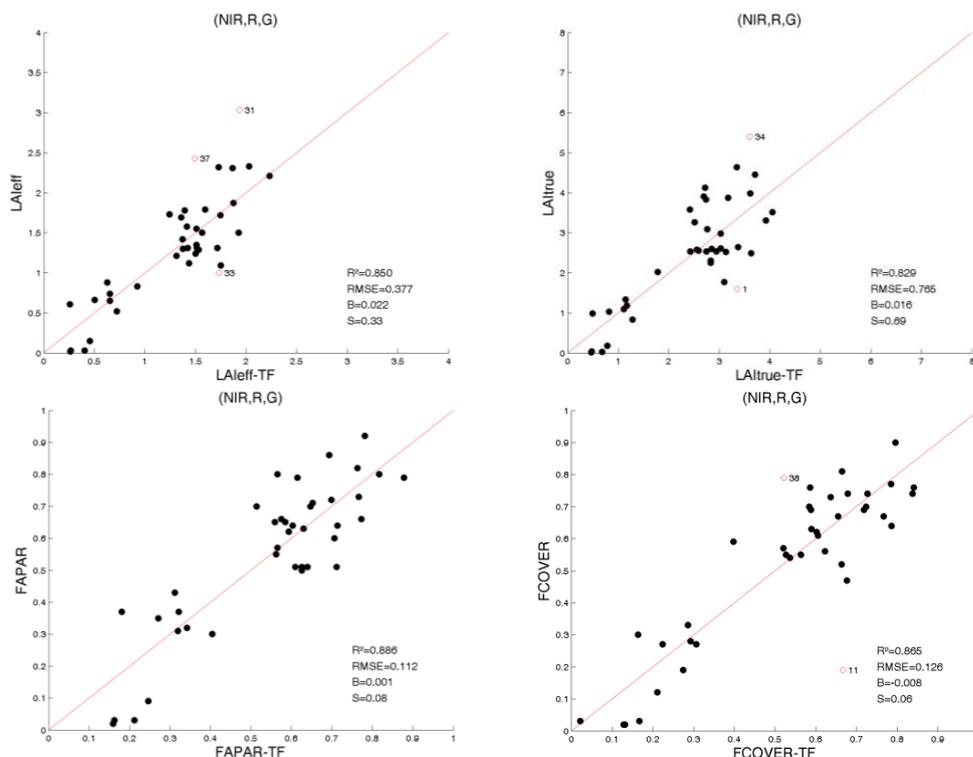
Figure 21: LAIeff, LAI, FAPAR and FCOVER results for regression on reflectance using 4 bands combination over Fasat-C image. Full dots: Weight>0.7. Empty dots: 0<Weight<0.7

6.3. THE HIGH RESOLUTION GROUND BASED MAPS

The high resolution maps are obtained applying the selected transfer function (Table 6) to the FASAT-C TOA reflectance. As the FASAT-C TOA was contaminated for some clouds, only the cloud-free 5x5 km^2 area is provided. Figure 22 shows the ground based maps provided for validation of satellite products at different spatial resolutions. Figure 19 shows the Quality Flags included in the final product.

FASAT-C maps. San Fernando site – Chile 19th January, 2015

LAIeff

LAI

FAPAR

FCOVER
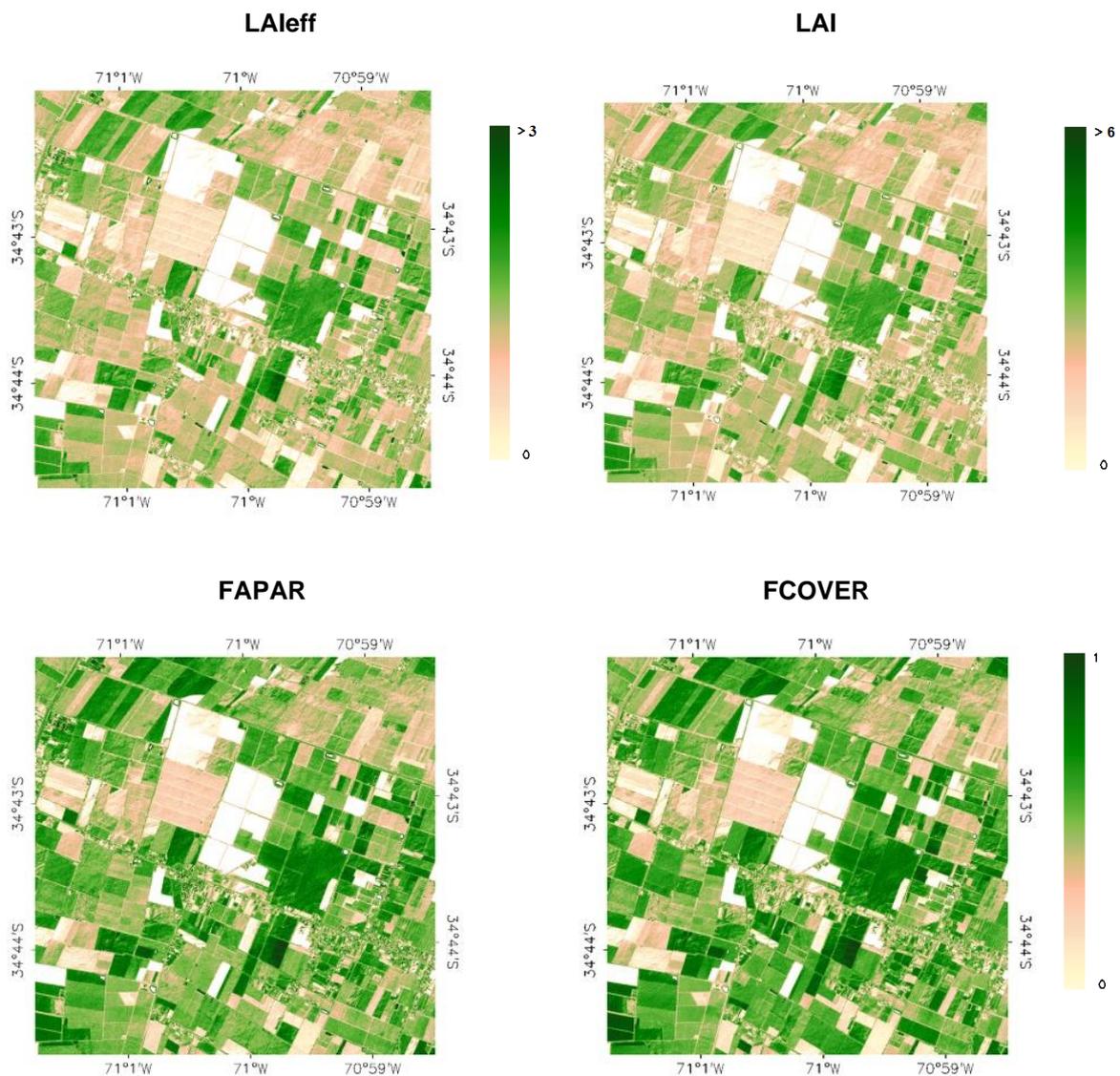
Figure 22: Ground-based maps (5x5 km^2) retrieved over FASAT-C image, on the San Fernando site (Chile), 19th January 2015.

Figure 23 shows the good consistency between the retrieved biophysical maps. The quality flag map has been taken into account for this evaluation to exclude those pixels were the transfer function behaves as extrapolator.
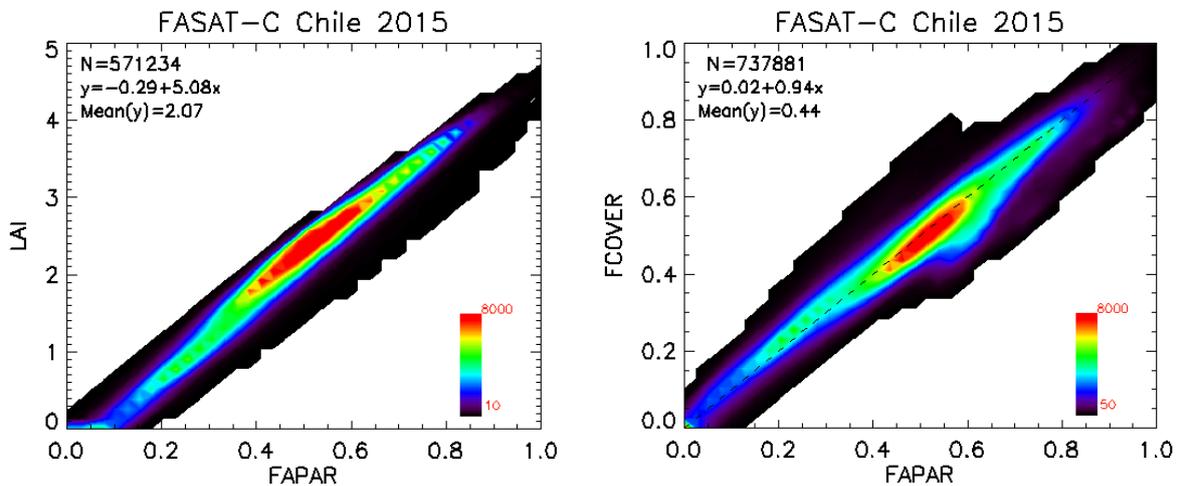
Figure 23: Scatter plots density between 5x5 km^2 maps. LAI versus FAPAR (Left) and FCOVER versus FAPAR (Right) retrieved over FASAT-C, San Fernando site (Chile), 19th January 2015.

6.3.1 Mean Values

Mean values of a 3x3 km^2 area centred in the test site are provided for validation of 1 km satellite products to reduce co-registration and PSF errors, and in agreement with the CEOS OLIVE direct dataset (Table 7). For the validation of coarser resolutions product (e.g. MSG products) a larger area should be considered. For this reason empirical maps are provided at 5x5 km^2.

Table 7: Mean values and standard deviation (STD) of the HR biophysical FASAT-C maps for the selected 3 x 3 km^2 area at San Fernando site (Chile).

FASAT-C - 3x3 km^2	LATITUDE	LONGITUDE
	-34.72275	-71.00190
	MEAN	STD
LAIeff	1.01	0.66
LAI	1.96	1.24
FAPAR	0.43	0.26
FCOVER	0.44	0.26

Table 8 describes the content of the geo-biophysical maps in the nomenclature: "BIO_YYYYMMDD_SENSOR_Site_ETF_Area" files, where:

BIO stands for Biophysical (LAIeff, LAI, FAPAR and FCOVER)

SENSOR = FASATC

YYYYMMDD = Campaign date

Site = San Fernando

ETF stands for Empirical Transfer Function

Area = 5x5 km^2

Table 8: Content of the dataset.

Parameter	Dataset name	Range	Variable Type	Scale Factor	No Value
LAI effective	LAIeff	[0, 7]	Integer	1000	-1
LAI	LAI	[0, 7]	Integer	1000	-1
FAPAR	FAPAR	[0, 1]	Integer	10000	-1
Fraction of Vegetation Cover	FCOVER	[0, 1]	Integer	10000	-1
Quality Flag	QFlag	0,1,2 (*)	Integer	N/A	-1

[*] 0 means extrapolated value (low confidence), 1 strict interpolator (best confidence), 2 large interpolator (medium confidence)

7. CONCLUSIONS

The FP7 ImagineS project continues the innovation and development activities to support the operations of the Copernicus Global Land service. One of the ImagineS demonstration sites is the San Fernando site in Chile. This site is located very close to the city of San Fernando.

This report presents the ground data collected during an intensive field campaign on 19th and 20th of January, 2015. The dataset includes 40 elementary sampling units where digital hemispherical photographs were taken and processed with the CAN-EYE software to provide LAI, LAIeff, FAPAR and FCOVER values to characterize the main crops in the study area. Two versions of CAN-EYE have been used to process the DHP, providing very consistent results except for FAPAR where the new version (v6.4) provides systematically lower values. Finally, the new version (v6.4) was selected as it allows a better identification of the shaded areas. Additional soil moisture measurements were also collected.

High resolution ground-based maps of the biophysical variables were produced over the site. Ground-based maps have been derived using high resolution imagery (FASAT-C TOA reflectance) according with the CEOS LPV recommendations for validation of low resolution satellite sensors. Transfer functions have been derived by multiple robust regressions between ESUs reflectance and the several biophysical variables. The spectral band combinations to minimize errors (weighted RMSE and cross-validation RMSE) were band 2 (green), band 3 (red), band 4 (Near Infrared) for all variables performed over the FASAT-C image.

The RMSE values for the several transfer function estimates are 0.377 for LAIeff, 0.765 for LAI, 0.11 for FAPAR, and finally 0.13 for FCOVER.

The quality flag maps based on the convex-hull analysis show a very good quality around the study area. The percentages for the FASAT-C transfer function of good interpolation capabilities for the 5x5 km^2 study area are higher than 77%.

The biophysical variable maps are available for the 5x5 km^2 area because the image presents some clouds over the site. They are provided in geographic (19 South UTM projection WGS-84) coordinates at 5.8 m resolution. Mean values and standard deviation over a validation area of 3x3 km^2 for LAIeff, LAI, FCOVER and FAPAR were computed centered at the validation test site.

8. ACKNOWLEDGEMENTS

9. REFERENCES

Baret, F. and Fernandes, R. (2012). Validation Concept. VALSE2-PR-014-INRA, 42 pp.

Camacho, F., Cernicharo, J., Lacaze, R., Baret, F., and Weiss, M. (2013). GEOV1: LAI, FAPAR Essential Climate Variables and FCOVER global time series capitalizing over existing products. Part 2: Validation and intercomparison with reference products. *Remote Sensing of Environment, 137: 310-329.*

Demarez, V., Duthoit, S., Baret, F., Weiss, M. and Dedieu, G. (2008). Estimation of leaf area and clumping indexes of crops with hemispherical photographs. *Agricultural and Forest Meteorology. I48, 644-655.*

Fernandes, R., Plummer, S., Nightingale, J., et al. (2014). Global Leaf Area Index Product Validation Good Practices. CEOS Working Group on Calibration and Validation - Land Product Validation Sub-Group. *Version 2.0.1: Public version made available on LPV website.*

Martínez, B., García-Haro, F. J., & Camacho, F. (2009). Derivation of high-resolution leaf area index maps in support of validation activities: Application to the cropland Barrax site. *Agricultural and Forest Meteorology, 149, 130–145.*

Mattar, C., Hernández, J., Santamaría-Artigas, A., Durán-Alarcón, C., Oliver-Guerra, L., et al. (2014). A first in-flight absolute calibration of the Chilean Earth Observation Satellite. *ISPRS Journal of Photogrammetry and Remote Sensing, 92:16-25.*

Miller, J.B. (1967). A formula for average foliage density. Aust. J. Bot., 15:141-144

Morisette, J. T., Baret, F., Privette, J. L., Myneni, R. B., Nickeson, J. E., Garrigues, S., et al. (2006). Validation of global moderate-resolution LAI products: A framework proposed within the CEOS land product validation subgroup. *IEEE Transactions on Geoscience and Remote Sensing, 44, 1804–1817.*

Latorre, C., Camacho, F., Pérez, Beget M.E. and Di Bella, C. (2014). "Vegetation Field Data and Production of Ground-Based Maps: 25 de Mayo site. La Pampa, ARGENTINA" report. 18 -20 (Available at ImagineS website: http://fp7-imagines.eu/pages/documents.php).

Weiss, M., Baret, F., Smith, G.J., Jonckheere, I. and Coppin, P., (2004). Review of methods for in situ leaf area index (LAI) determination. Part II. Estimation of LAI, errors and sampling. *Agricultural and Forest Meteorology. 121, 37–53.*

Weiss M. and Baret F. (2010). CAN-EYE V6.1 User Manual

Welles, J.M. and Norman, J.M., 1991. Instrument for indirect measurement of canopy architecture. Agronomy J., 83(5): 818-825.